Flow and Dispersion in Porous Media: Lattice-Boltzmann and NMR Studies

B. Manz and L. F. Gladden
Dept. of Chemical Engineering, University of Cambridge, Pembroke Street, Cambridge CB2 3RA, U.K.

P. B. Warren
Unilever Research Port Sunlight Laboratory, Bebington, Wirral L63 3JW, U.K.

The results of lattice-Boltzmann simulations of the flow field through a random packing of spheres are compared with NMR velocimetry and propagator measurements. Flows are investigated for Péclet (Pe) and Reynolds (Re) numbers in the range $182 < Pe < 350$ and $0.4 < Re < 0.77$, respectively. An MRI visualization of the 3-D packing of spheres for which NMR data are obtained is used as the matrix for the simulation, thereby enabling a direct assessment of the ability of the lattice-Boltzmann method to quantitatively predict flow phenomena within porous media of complex geometry. By introducing normalized parameters, hydrodynamical dispersion over normalized displacement lengthscales extending over nearly four orders of magnitude is investigated and is shown to be dominated by mechanical dispersion over most of this range. At the largest lengthscales studied holdup may play a significant role in the hydrodynamics characteristic of the porous medium. Quantitative agreement between NMR measurements and the predictions of the lattice-Boltzmann simulation is obtained in all cases.

Introduction

In recent years, the lattice-Boltzmann method (Higuera and Jiménez, 1989) has been extremely successful in simulating fluid flows. The method has been evaluated by simulating flow in simple 2-dimensional (2-D) and 3-dimensional (3-D) geometries and comparing the results to those obtained from experiments and other simulation methods (Chen and Doolen, 1998, and references therein). More complex problems include the simulation of Rayleigh-Bénard convection (Shan, 1997), multicomponent flow (Shan and Chen, 1993; Martys and Chen, 1996), and the flow of non-Newtonian fluids (Aharanov and Rothman, 1993; Gonnella et al., 1997). Diffusion and hydrodynamic dispersion have been simulated using the lattice-Boltzmann method for pipe flow (Calì et al., 1992) and around a stagnation point in a Hele-Shaw cell (Flekkøy et al., 1995). With the so-called moment propagation method (Frenkel and Ernst, 1989; Lowe and Frenkel, 1995) it is possible to simulate hydrodynamic dispersion in complex systems. Of particular interest for engineering applications is the understanding of fluid flow in porous media. Model porous media have been created using computer simulations, which were then taken as the simulation lattice upon which to investigate permeability (Heijs and Lowe, 1995; Spaid and Phelan, 1997) and velocity distribution functions (Maier et al., 1998) using the lattice-Boltzmann method. To date, there have been no comparisons between lattice-Boltzmann simulations and measured flow fields in the same porous sample. The aim of this work is to perform an assessment of the ability of the lattice-Boltzmann method to predict quantitatively the characteristics of fluid flow in porous media.

An ideal, noninvasive tool for the investigation of fluids in porous media is nuclear magnetic resonance (NMR). In particular, magnetic resonance imaging (MRI) is used to obtain the spatially resolved distribution of a range of physical parameters in two or three dimensions (Callaghan, 1991), such as the density distribution of a fluid (in the present case water) filling the pore space. A 3-dimensional volume image obtained in this way can then be analyzed to obtain characteristics of the void space and of the individual pores within the void space (Baldwin et al., 1996). Furthermore, spatially resolved NMR velocimetry gives the fluid-velocity distribution in the pore space (Guilfoyle et al., 1992; Chen et al.,

Correspondence concerning this article should be addressed to L. F. Gladden.
Current address of P. B. Warren: Unilever Research Port Sunlight Laboratory, Quarry Road East, Bebington, Wirral L63 3JW, U.K.

1993; Kutsovsky et al., 1996; Mansfield and Issa, 1996; Sederman et al., 1997). Spatially nonresolved probability distributions of molecular displacements can be measured using the pulsed-gradient spin echo (PGSE) NMR (Stejskal and Tanner, 1965) technique. By following the time dependence of these probability distributions, one can probe the pore space on spatial and temporal resolutions not accessible with MRI (Lebon et al., 1996, 1997; Seymour and Callaghan, 1996, 1997; Packer and Tessier, 1996; Amin et al., 1997; Tessier et al., 1997; Manz et al., 1999).

In this study we report the measurement and lattice-Boltzmann simulation of fluid flow in model porous media. The results of lattice-Boltzmann simulations of the flow field through a random packing of spheres of diameter 1 mm are compared directly with NMR velocimetry measurements. An MRI visualization of the 3-D packing of spheres for which NMR velocimetry data are obtained is used as the matrix for the simulation. This approach enables an assessment of the ability of lattice-Boltzmann to quantitatively predict flow phenomena within porous media of complex geometry, since the experimental measurement of the flow characteristics and the simulations are performed on exactly the same porous structure. Further, comparison is made between the predictions of the lattice-Boltzmann simulations and the displacement variance (that is, dispersion) characteristic of the fluid moving within the pore space for three sphere packs composing spheres of diameter 1 mm, 0.5 mm and 0.1 mm, respectively. Excellent agreement is found between experimental results and the simulations for the normalized displacement variance in both axial and transverse directions. By introducing normalized parameters, hydrodynamical dispersion over normalized displacement lengthscales extending over nearly four orders of magnitude is investigated. Comparison of the experimental data with lattice-Boltzmann simulations considering different values of the fluid self-diffusivity has allowed us to investigate the lengthscales over which mechanical dispersion dominates the hydrodynamics of the system. We conclude that at the largest lengthscales studied holdup may play a significant role in the hydrodynamics characteristic of the porous medium. Quantitative agreement between NMR measurements and the predictions of the lattice-Boltzmann simulation is obtained in all cases.

The article is organized as follows. First a brief description of the lattice-Boltzmann method, followed by an overview of some theoretical concepts regarding dispersion in porous media is given. The following section describes the experimental methods used to characterize the pore space and the fluid flow therein. Finally, the results of the lattice-Boltzmann simulations and magnetic resonance flow visualization and dispersion measurements are presented and discussed.

The Lattice-Boltzmann Method

On a microscopic scale, the particles in a simple fluid, at equilibrium, in the bulk phase move in all directions with equal probability. In numerical simulations of the same process, in which this motion is constrained on a coarse grid, or lattice, of low rotational symmetry it is not immediately obvious that the hydrodynamic isotropy is still conserved. However, Frisch et al. (1986), using a lattice gas automaton (LGA) approach showed that this can indeed be achieved using a simple hexagonal 2-dimensional grid. More recently, other grids with m base vectors have been designed in 2, 3, and 4 dimensions. The particles in such an LGA are located on the lattice sites and are allowed to move with a fixed speed along the directions of the lattice vectors c_i, $i = 1, \ldots, m$. Collisions may occur between particles at the same lattice site. These collisions have to conserve both mass and momentum. The particle dynamics can be expressed by the following equation:

$$n_i(x + c_i, t+1) = n_i(x,t) + \Delta[n(x,t)].$$

Here the time t is integer-valued and the duration of the time step is taken to be unity. The state variables n_i are Boolean variables indicating the presence ($n_i = 1$) or absence ($n_i = 0$) of particles moving from a lattice site at position x to the neighboring site at $x + c_i$. The function Δ_i is called the collision operator and can take on the values 0 and ± 1. A detailed description of the LGA model is given by Rothman and Zaleski (1997). A major drawback of the LGA approach is that it requires extensive ensemble averaging or time averaging to produce statistically significant results. The lattice-Boltzmann method overcomes this problem by ensemble averaging over the microstates of the lattice gas, thereby obtaining a coarse-grained description of the time evolution of the lattice gas, analogous to the Boltzmann equation for a dilute gas, but discretized in space, time, and velocity (Higuera and Jiménez, 1989). Therefore, it is possible to simulate the motion of a fluid by following the time evolution of one-particle distribution functions N_i, which describe the number of particles at a lattice node x at time t with velocity c_i (Chen et al., 1992; Kingdon et al., 1992). Only a finite set of c_i is possible; the magnitudes and directions of the c_i are such that particles remain on lattice nodes during the discrete time evolution. The mass density ρ, momentum density ρu, and stress σ are given by

$$\rho = \sum_i N_i, \qquad \rho u = \sum_i N_i c_i, \qquad \sigma = \sum_i N_i c_i c_i.$$

The dynamics of these distribution functions in the single relaxation time scheme, is given by

$$N_i(x + c_i, t+1) = N_i(x_i, t) - \frac{1}{\tau}\left(N_i(x_i,t) - N_i^{(\mathrm{eq})}(x_i,t)\right)$$

where $N_i^{(\mathrm{eq})}$ is the pseudo-equilibrium distribution function. In a widely used class of models (Qian et al., 1992), the kinematic viscosity, υ, is related to the relaxation time for convergence, τ, by

$$\upsilon = (2\tau - 1)/6.$$

The simulations described in this article were performed using the double relaxation time scheme (Behrend et al., 1994) in the D3Q15 model (Warren, 1997). The D3Q15 model is based on a 3-D cubic lattice; it possesses a rest particle state, six links with nearest neighbors, and eight links with next-nearest neighbors. The relaxation time was set as $\tau = 0.75$, yielding a kinematic viscosity $\upsilon = 1/12$. Periodic boundary

conditions in the flow direction with bounceback on the solid nodes were used and, in order to drive the flow, a pressure difference was imposed between the two faces normal to the axis of the superficial flow by applying a uniform body force to the fluid (Ladd, 1994). The simulation was performed for Stokes flow, and the $N_i(x,t)$ were allowed to equilibrate for 30,000 iterations, which ensured steady-state conditions in the simulation. To obtain the propagators, the displacement of particles placed on lattice nodes in 20 slices (equivalent to about 2 sphere diameters) was traced. The first slice on which the particles were placed was located 10 pixels downstream from the upper surface of the simulation lattice. If a particle hits a solid boundary as the flow develops, the particle is allowed to diffuse until it returns to the flow field again—the length scale of any such diffusion is usually less than one pixel. The resolution of the lattice was made to be the same as that acquired in the image, thereby yielding a size for the 1-mm spheres equivalent to 11.6 lattice units. Designing the visualization and simulation to have the same resolution allows direct comparison of the predicted flow characteristics with experimental observation; this level of resolution also represents the highest resolution possible for the imaging experiment (given practical considerations) and the limit of computer memory when performing the simulations.

Dispersion in Porous Media

The basic concept used in describing the process of dispersion in porous media is the existence of a hierarchy of scales over which transport occurs (Cushman, 1990). Because it is not possible to obtain an exact mathematical description of the motion of each fluid element, it is common to solve the volume-averaged form of the transport equation (Paine et al., 1983). In the long-time limit this ''macro transport'' equation for the average concentration $\langle c\rangle$ of a tracer takes on the form of a macroscopic Fick's law with a constant effective dispersion tensor D^*:

$$\frac{\partial\langle c\rangle}{\partial t} + V\cdot\nabla\langle c\rangle = \nabla\cdot(D^*\cdot\nabla\langle c\rangle),$$

where the time-averaged velocity V is defined as

$$V = \lim_{t\to\infty}\frac{d\langle r(t)\rangle}{dt}.$$

D^* is then given by the autocorrelation function of the fluctuation $u(t) = v(t) - V$ in the velocity field $v(t)$:

$$D^* = \lim_{t\to\infty}\int_0^t \langle u(0)u(t')\rangle dt' = \lim_{t\to\infty}\frac{1}{2}\frac{d\sigma^2(t)}{dt},$$

where $\sigma^2(t) = \langle(r(t) - \langle r(t)\rangle)^2\rangle$ is the positional variance.

For flow in a fixed bed of spheres, an asymptotic analysis of D^* has been carried out by Koch and Brady (1985). It was found that in the long-time limit the behavior of D^* can be described by the Péclet number $Pe = v_{ave}d/D_s$, where v_{ave} is the volume-averaged fluid velocity in the pore space, d is the sphere diameter, and D_s is the fluid self-diffusivity. Three principal processes for the scaling of D^* with Pe can be distinguished. Mechanical dispersion arises from the stochastic variations of the velocity field due to the arrangement of the pores and scales with Pe. Taylor dispersion (Taylor, 1953) scales with Pe^2 and is due to the diffusion of fluid molecules across streamlines. The presence of blocked pores causes holdup dispersion, which scales as $Pe\log(Pe)$. It has been shown in the literature that in the range $10 < Pe < 300$, D^* scales as Pe^{α}, where α is around 1.1–1.3 (Seymour and Callaghan, 1997, and references therein; Manz et al., 1999), indicating that in this range the structure of the pore space dominates the dispersion behavior, although diffusion cannot be neglected. This regime is termed the boundary-layer diffusion regime by Koch and Brady (1985). If the lengthscales and time scales on which transport occurs are not much larger than the scale of the fluctuations in the velocity field, the description in terms of local, averaged transport equations is not applicable. For such cases, a nonlocal transport theory has been developed by Koch and Brady (1987). Other more accurate models have also been reported (Cushman, 1997), but a detailed comparison of the experimental data with these models is considered beyond the scope of this article.

In recent years the simulation of flow and dispersion in porous media using the lattice-Boltzmann method has been very successful. Calì et al. (1992) performed lattice-Boltzmann simulations of self-diffusion in 2-D fractal structures. The mean-square displacement from the origin $R^2(t)$ of a point particle undergoing random motion in such a structure scales as $R^2(t) \sim t^{2\upsilon}$, with the exponent $\upsilon < 0.5$. It was found that the exponent obtained from the simulation agreed well with that calculated analytically. Lattice-Boltzmann simulations of the velocity autocorrelation function of fluid flow in porous media using the moment propagation method (Frenkel and Ernst, 1989; Lowe and Frenkel, 1995) showed evidence that the dispersion coefficient is diverging at Péclet numbers $Pe > 600$ (Lowe and Frenkel, 1996). Axial and transverse dispersion coefficients have been modeled in 3-D fractal structures using the method of moments and random walks (Salles et al., 1993). Good agreement was found with the analytical results obtained using the theory by Koch and Brady, discussed earlier. Georgiadis et al. (1996) have applied lattice-Boltzmann simulations to study steady flow driven by a uniform pressure gradient through a computer-generated packing of spheres at solids fractions in the range 10–62%. Their results reproduced the exponential distribution of velocity in the direction of superficial flow previously observed by Lebon et al. (1996) and Kutsovsky et al. (1996). More recently, further lattice-Boltzmann simulations employing computer-generated 3-D packings of particles have been reported. In particular, axial velocity distribution functions (Maier et al., 1998) have been presented. By comparing the simulated axial velocity distribution functions to experimental results obtained by PGSE NMR it was found that the lattice-Boltzmann simulation overpredicts the probability distribution at high velocities, while low velocities are underpredicted.

In this article we will use the 3-D NMR image of a porous medium as the lattice with which to simulate the flow field. These velocity profiles are then compared to NMR velocimetry measurements obtained on the same bed. The time-

dependence of the bulk-displacement distribution functions is also calculated for displacements ranging between 0.01 and 100 sphere diameters. Briefly, putting the present study in the context of earlier work, we note that Lebon et al. (1997) considered flow through a nonconsolidated packing of spheres, with spheres in the range 81–800 μm; mean displacements between 0.1 and 7.3 bead diameters were investigated, and the main features of the propagator measurements were reproduced by a Monte Carlo model based on a random-pore network representation of the porous medium. Packer and coworkers (such as Packer and Tessier, 1996; Tessier et al., 1997) have reported a number of experimental studies and also some comparisons with numerical predictions. In particular, Tessier et al. (1997) report flow through Fontainebleau sandstone and a packing of 3-mm-diameter spherical beads. Representative structures of these porous media were computer-generated and the flow fields simulated, from which the propagators were derived by solving the Stokes equations within these structures. In the case of flow through the sphere packing, mean displacements up to 50 sphere diameters were probed and a comparison with the numerical prediction of the propagators was given. Other workers have reported purely experimental pulsed-gradient spin echo studies. In particular, Seymour and Callaghan (1997) have reported experiments, probing mean displacements of approximately 3 bead diameters, for a packing of 90.7-μm-diameter polystyrene latex spheres, while Amin et al. (1997) considered 300-μm beads and probed mean fluid displacements up to 60 bead diameters. Our work describes the first combined experimental and numerical study in which the simulated flow field and propagators, and the experimental data are all produced for exactly the same porous structure. Further this is the first report of predictions of the time evolution of the flow propagator using the lattice-Boltzmann technique and their comparison with experimental data.

NMR Measurements of Fluid Density and Displacements

The imaging of the fluid density $\rho(r)$ and velocity $v(r)$ distributions is performed by Fourier encoding using radio frequency (rf) and magnetic-field gradient pulses. A detailed description of these techniques is given by Callaghan (1991); here we outline the principles of the techniques used.

A timing diagram of the rf and magnetic-field gradient pulses for obtaining a 3-D image of the fluid density distribution is shown in Figure 1. A reciprocal space vector k can be defined as

$$k = \frac{1}{2\pi}\gamma G t,$$

where $\gamma = 2.68\times10^{8}\ \mathrm{T\cdot m^{-1}}$ is the gyromagnetic moment of the hydrogen nucleus, and G is the vector of the magnetic-field gradient. The resulting NMR signal $S(k)$ is then modulated by k and is given by

$$S(k) = \int \rho(r)\exp(i2\pi k\cdot r)\ dr.$$

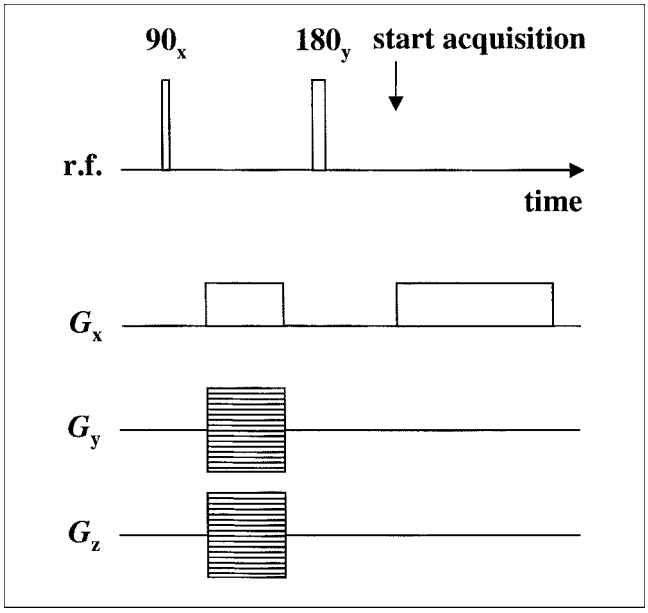

Figure 1. rf and gradient pulse sequence used for a 3-D image of the pore space.

The fluid density distribution is obtained by Fourier inversion:

$$\rho(r) = \int S(k)\exp(-i2\pi k\cdot r)\ dk.$$

The spin density images acquired using this spin-echo pulse sequence are then binary gated in order to obtain a three-dimensional map of the pore space.

Molecular displacements are measured using the pulsed-gradient spin echo (PGSE) (Stejskal and Tanner, 1965) or stimulated echo (PGSTE) (Tanner, 1970) sequences. These sequences provide the bulk-displacement probability distributions over a time Δ. A matched pair of magnetic-field gradient pulses of duration δ, strength g, and separation Δ, is applied along with a sequence of rf pulses, as shown in Figure 2a. In the narrow-gradient pulse approximation ($\delta \ll \Delta$), the first gradient imparts a phase shift $\phi(r) = \gamma\delta g\cdot r$ to a spin at position r. This phase shift is inverted by the following two 90° rf pulses. If the molecule carrying the spin has moved from r to r' during the time Δ, the net phase shift following the second gradient pulse is $\phi(r) = \gamma\delta g\cdot(r' - r)$. Defining a dynamic displacement $R = r' - r$ and the average displacement propagator $\bar{P}_S(R,\Delta)$ as the average probability that any molecule in the sample will move by a dynamic displacement R over time Δ, the normalized echo signal is given by

$$E(q,\Delta) = \int \bar{P}_S(R,\Delta)\exp(i2\pi q\cdot R)\ dR,$$

where $q = (1/2\pi)\gamma\delta g$ is the reciprocal displacement vector (Kärger and Heink, 1983), and q is the amplitude of q. We remark that in the language of kinetic theory, $E(q,\Delta)$ is known as the self-dynamic structure factor. In the following

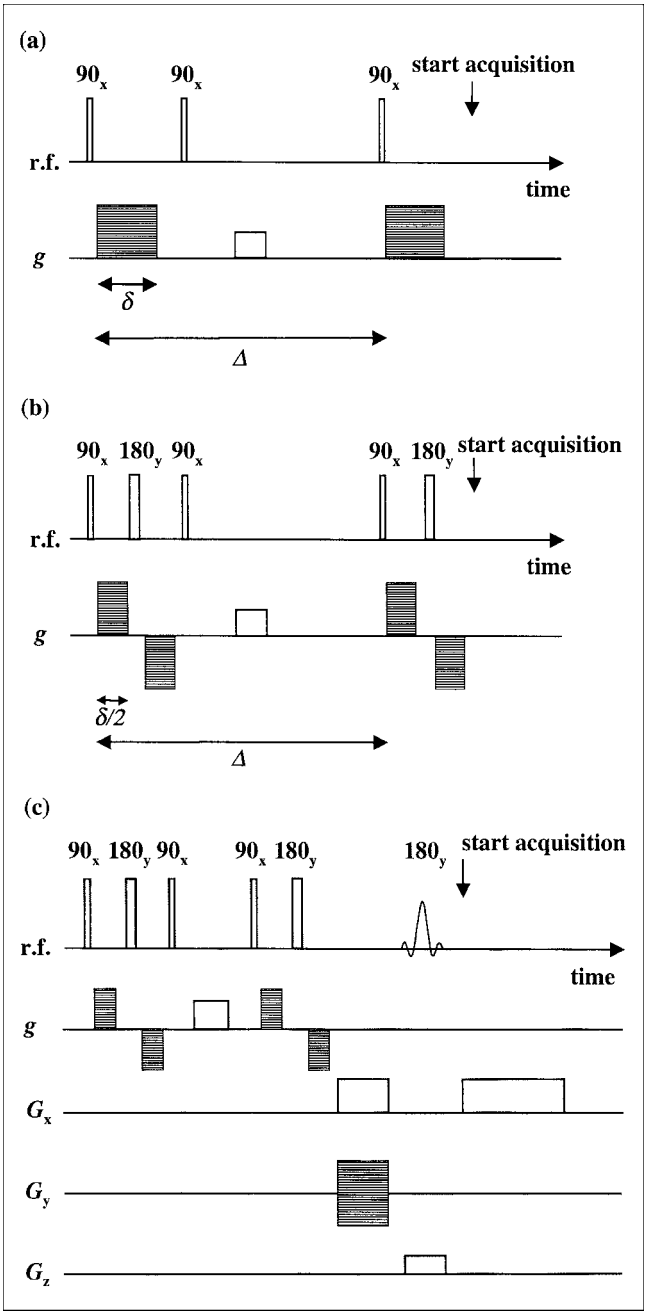

Figure 2. PGSTE (a) and APGSTE (b) pulse sequences for measuring molecular displacements.

The APGSTE pulse sequence minimizes signal loss due to magnetic susceptibility effects. In (c), the diagram of a pulse sequence for measuring a spatially resolved velocity map in a 2-D slice is shown.

analysis we will only consider displacements R along the direction of the magnetic-field gradient, which may be along the direction of the net flow or transverse to it. Hence $\bar{P}_S(R,\Delta)$ can be obtained by the measurement of $E(q,\Delta)$ and subsequent Fourier inversion with respect to q. The net effect of the PGSTE experiment is to effectively tag molecules by manipulation of their nuclear spin, and this distribution can then be probed at later times. The experiment is therefore equivalent to one in which a tracer is introduced into the flow and the average distribution of the tracer from its initial location is determined in a completely noninvasive manner. By varying the observation time Δ, one can follow the time evolution of the displacement propagator from a ''snapshot'' velocity propagator (short Δ) to an average propagator over long time periods (long Δ). During these time scales the propagator samples structural features over different length-scales within the medium, thus enabling us to determine the lengthscales that govern the hydrodynamics inside a complex pore space. In porous media, the variation of the magnetic field due to the difference in magnetic susceptibility between liquid and solid matrix leads to a rapid decay in the NMR signal. The alternating PGSTE (APGSTE) pulse sequence, which is shown in Figure 2b, uses spin echoes to minimize this effect (Cotts et al., 1989).

The techniques for measuring the fluid density and displacement propagator can be combined in order to obtain spatially resolved maps of molecular displacements. The pulse sequence used in the experiments reported here is shown in Figure 2c. Note that now a 2-D slice is imaged. The acquired signal, $S(k,q)$, is now modulated by the two wave vectors k and q, and is given by

$$S(k,q) = \int \rho(r) \exp(i2\pi k\cdot r) \int P_S(r|r+R,\Delta) \exp(i2\pi q\cdot R)\, dr\, dR,$$

where $P_S(r|r+R,\Delta)$ represents the probability that a spin, which is located at r at $t=0$ moves to $r+R$ at time Δ. Fourier inversion yields

$$P_S(r|r+R,\Delta) = \frac{\iint S(k,q)\exp(-i2\pi k\cdot r)\exp(-i2\pi q\cdot R)\, dk\, dq}{\int S(k,0)\exp(-i2\pi k\cdot r)\, dk}$$

From this displacement propagator, which is now averaged over a single image voxel, one can calculate the mean fluid displacement $Z(r)$ along the direction of q. The mean velocity $\bar{v}(r)$ is then given by $\bar{v}(r) = (Z(r)/\Delta)$. By keeping the observation time short compared to the time scales over which velocity fluctuations occur, one can obtain a velocity ''snapshot'' image. Steady-state conditions are required for the duration of data acquisition, which was in this case is 2 hours.

Experimental Details

The model porous media investigated in this work were three unconsolidated packings of glass spheres of different diameters contained within a glass column. Because the nature of the packing depends on the particle diameter-to-column ratio, three columns of different diameters were used in order to keep this ratio approximately constant. The parameters for each sample are given in Table 1. Each packing formed a column length of 6 cm. In order to reduce the longitudinal relaxation time of the water protons, and thereby

Table 1. Parameters Describing Each of the Three Samples Used in this Study

Sample	Sphere Dia. (mm)	Column Dia. (mm)	v_{ave} (mm s^{-1})	*Pe*	*Re*
1	1.0	10	0.77	350	0.77
2	0.5	4	0.80	182	0.4
3	0.1	1.3	4.4	200	0.44

enabling more rapid data acquisition, a l-mM aqueous $CuSO_4$ solution was used as the flow liquid. A constant flow rate through the packing was achieved by using a Harvard Apparatus (South Nattick, MA) syringe pump. The volumetric flow rates were in the range of 4–100 mL·h^{-1}, corresponding to mean interstitial velocities of 0.77–4.4 mm·s^{-1}. The corresponding Péclet numbers range from 180 to 350, while the Reynolds numbers are less than unity (see Table 1). These experimental conditions were selected such that the dispersion process was expected to be dominated by the structure of the pore space (mechanical dispersion), and inertial effects in the flow field were small; that is, experiments are performed in the creeping flow regime. The packings were aligned with the direction of the net flow, along the axis of the magnet. NMR experiments were performed on a Bruker DMX 200 spectrometer with a microimaging probe. The maximum field gradients achievable were 1.6 T·m^{-1} and 0.49 T·m^{-1} in the axial and transverse directions, respectively.

For sample 1 it was possible to measure both a 3-D image of the fluid density distribution and a 2-D velocity map through a thin central slice. The 3-D image was obtained at zero flow using the 3-D imaging pulse sequence shown in Figure 1 with a cubic voxel resolution of $(0.086\ \text{mm})^3$. The image was then gated to produce a binary image representing void space and glass spheres, which was used as the matrix for the lattice-Boltzmann simulation. The velocity map was measured using the pulse sequence shown in Figure 2c. A slice of 0.5 mm thickness was imaged with a voxel resolution of $(0.086\ \text{mm})^2$ in the imaging plane. The fluid velocities were imaged in all three spatial directions with a velocity resolution of 0.15 mm s^{-1}. The displacement propagators $\bar{P}_S(R, \Delta)$ were obtained by Fourier inversion of $E(q, \Delta)$, which was measured with q gradients applied along and transverse to the net flow direction using the 13-interval APGSTE pulse sequence (Cotts et al., 1989), which is shown in Figure 2b. The gradient pulse duration $\delta/2$ was held constant during each experiment and g was incremented in 128 equal steps between 0 and g_{max}. In order to avoid signal aliasing, the values of $\delta/2$ and g_{max} were adjusted separately for each sample and delay time Δ. Eight-step phase cycling described by Amin et al. (1997) with a relaxation delay of 2 s was applied. For samples 2 and 3 only displacement propagators were measured; full flow visualization data were not recorded.

Comparison of Experimental Results and Lattice-Boltzmann Simulations

In Figure 3 the experimental fluid velocity maps are shown for all three velocity components along with the corresponding lattice-Boltzmann simulation for the same transverse slice. In presenting this comparison, it is important that the spatial resolutions associated with the MRI visualization and lattice-Boltzmann predictions are comparable. The in-plane resolution of the MRI flow visualization experiment is 0.086 mm and the image slice thickness is 0.5 mm. The spatial resolution of the lattice-Boltzmann simulation is 0.086 mm; hence, to obtain a quantitative comparison between experiment and simulation it was necessary to average over six transverse layers in the simulation results. Further, comparison between the results of the lattice-Boltzmann simulation and the experimental data is made subject to the mean flow velocity predicted by the simulation being set equal to that determined experimentally. Given that we are considering Stokes flow, this is equivalent to adjusting the pressure difference across opposite faces of the simulation lattice. The overall agreement between experiment and simulation is excellent. Qualitatively, all the features in the experimental velocity maps are reproduced by the simulation.

For a more quantitative analysis, we subtracted the predicted from the experimentally determined velocities for each image pixel. This difference map is shown in the righthand column of Figure 3. Although the qualitative agreement between experiment and simulation is very good, there are differences in the velocity maps that cannot be attributed to noise in the experiment. In general, the lattice-Boltzmann simulation overpredicts large axial velocities, while low axial velocities are underpredicted. Standard deviations calculated from the difference images in Figure 3 are 0.44, 0.42, and 0.59 mm s^{-1} for the *x*-, *y*-, and *z*-components of the velocity vector, respectively.

Given the good agreement between experimental velocity profiles and the lattice-Boltzmann simulation, it is of interest to investigate whether the simulation is also able to predict the bulk-displacement probabilities $\bar{P}_S(R, \Delta)$. The simulated displacement propagators were calculated from the 3-D velocity simulation by tracing a representative number of fluid particles starting at the lattice nodes, as described earlier, in discrete time steps of duration $dt = 0.1$ ms over the time Δ. Time steps smaller than 0.1 ms were considered in preliminary simulations and found to converge to the same results as those for a time step of 0.1 ms, which was therefore chosen to minimize computation time. Self-diffusion was simulated by imposing random jumps with a Gaussian probability distribution on top of the pressure-driven flow. In each spatial direction the variance of the jump length was $2\ D_s dt$, where D_s is the fluid self-diffusivity, and the mean jump length was zero. The value of the self-diffusivity of water at 296 K, the temperature at which the experimental data were recorded in this study, was taken as $D_s = 2.2 \times 10^{-9}$ m^2·s^{-1} (Mills, 1973). A comparison between experimental displacement propagators and the simulations at different times Δ is shown for sample 1 along, and transverse to, the direction of the net flow in Figures 4 and 5, respectively. Overall, the quantitative agreement is again very good, although there are differences in some details.

Inspection of the propagators along the axial direction in Figure 4 shows that low velocities, especially around the peak, are underpredicted by the simulation, whereas high velocities are slightly overpredicted. These observations are consistent with the work of Maier et al. (1998). This effect is reversed for displacements in the transverse direction, as can be seen from Figure 5. Here, the simulation overpredicts the peak at

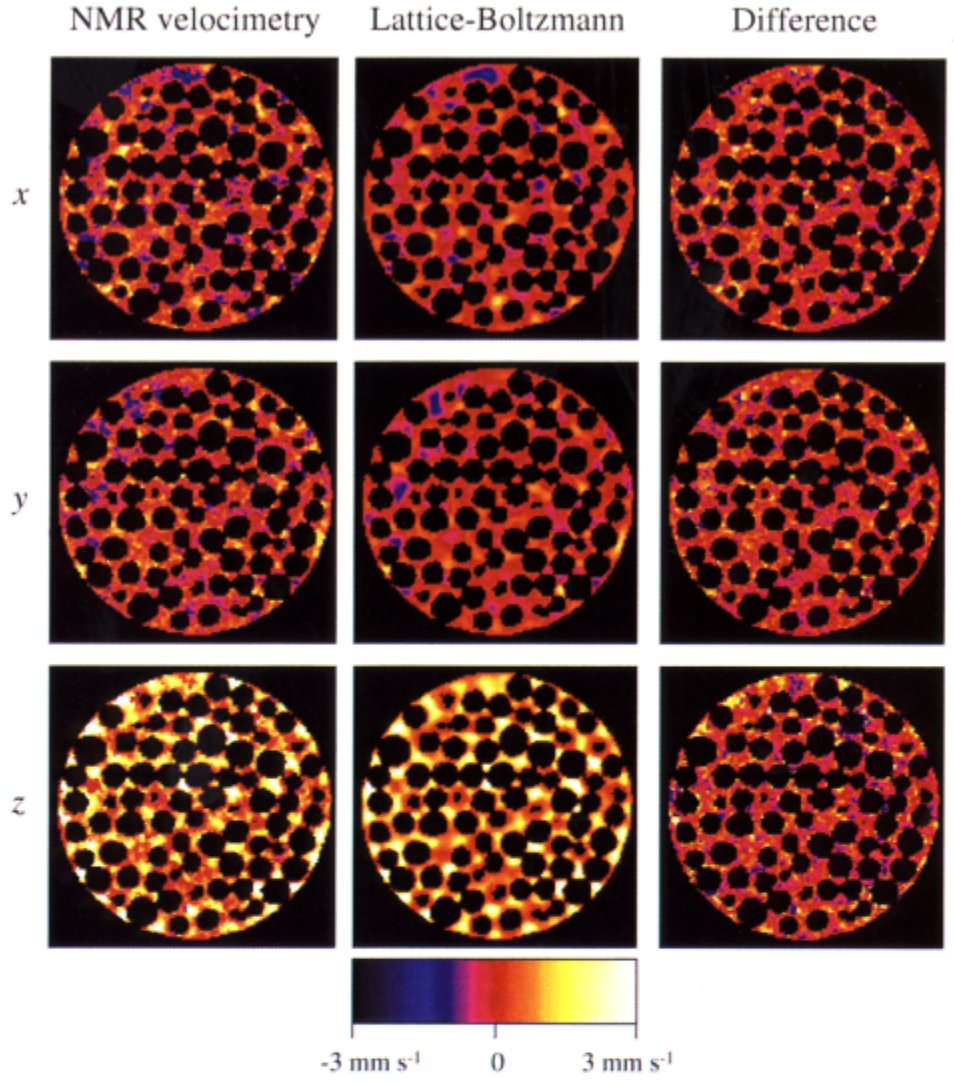

Figure 3. NMR velocimetry measurements (left) vs. lattice-Boltzmann simulations (middle) of fluid flow through a transverse slice of sample 1.

The velocity components along the x, y, and z directions are shown, z being the direction of superficial flow. Difference maps obtained by subtracting the lattice-Boltzmann map from the MRI visualization are shown in the right-hand column, for each of the velocity components.

zero displacement, and at all times the simulated curves fall off more rapidly than the experimentally determined propagators. The systematic difference between the measured and simulated flow fields might be accounted for in the fact that we only simulated Stokes flow and therefore did not include the inertial term in the Navier-Stokes equation in the lattice-Boltzmann simulations presented here. Differences between our predictions and experimental data could also arise from discretization error. A detailed consideration of these effects is the subject of ongoing work.

In a recent study (Manz et al., 1999), we used the displacement propagators to calculate the average displacement variance $\sigma^2(t)$, which is a measure of hydrodynamic dispersion. In the following discussion only the relevant results from that earlier work are reported; the reader is referred to our previous work for a detailed discussion of the form of the observed propagators. As stated earlier, for the range of Péclet numbers considered in this study, dispersion is expected to be dominated by the structure of the medium (mechanical or convective dispersion), although diffusion cannot be neglected. Therefore, it is appropriate to consider the normalized average displacement variance σ^2/d^2 as a function of the normalized average axial displacement $\zeta = v_{ave}\Delta/d$. In Figure 6, these experimental data are shown for displacement in the axial and transverse directions for all three samples studied, along with the results of the lattice-Boltzmann

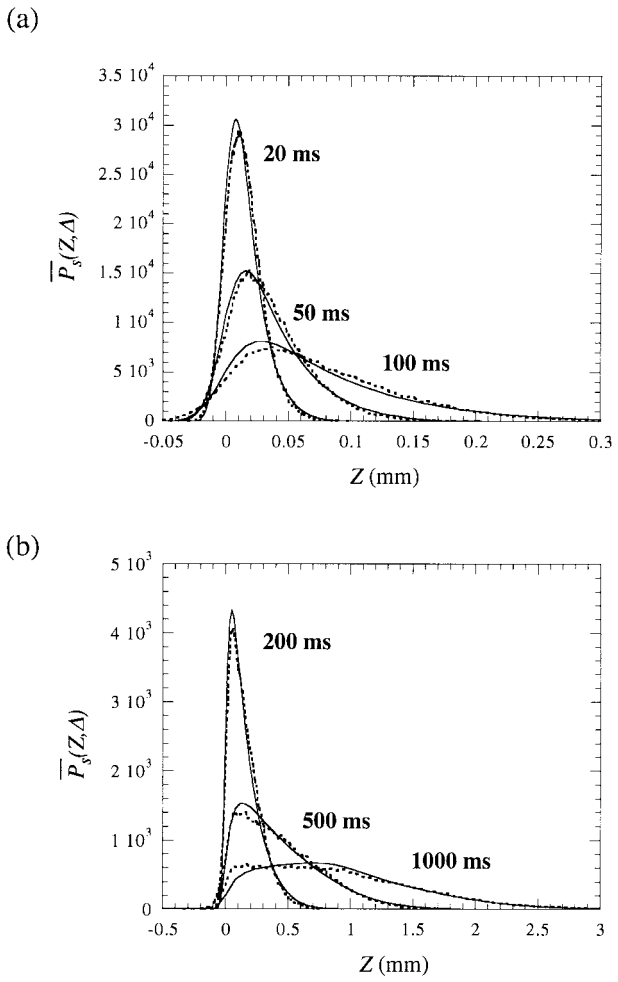

Figure 4. Experimental (——) vs. simulated (– – –) displacement propagators along the axial direction for varying values of Δ: (a) Δ = 20, 50, 100 ms; (b) Δ = 200, 500, 1,000 ms.

Note the change in scaling between (a) and (b). Data are shown for sample 1. The mean displacement (mm) values calculated from the experimental and predicted propagators [reported as (experimental:simulated)] for each propagator are: Δ = 20 ms [0.0146:0.0147]; Δ = 50 ms [0.032:0.034]; Δ = 100 ms [0.073:0.075]; Δ = 200 ms [0.151:0.152]; Δ = 500 ms [0.434:0.429]; Δ = 1000 ms [0.903:0.877].

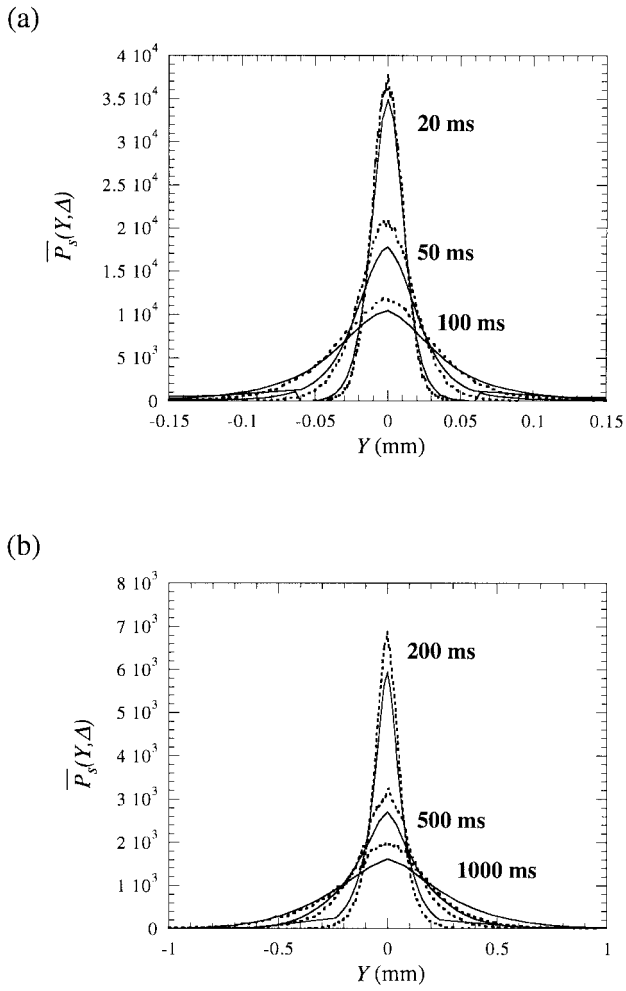

Figure 5. Experimental (——) vs. simulated (– – –) displacement propagators along the transverse direction for varying values of Δ: (a) Δ = 20, 50, 100 ms; (b) Δ = 200, 500, 1,000 ms.

Note the change in scaling between (a) and (b). Data are shown for sample 1. The mean displacement (mm) values calculated from the experimental and predicted propagators [reported as (experimental:simulated)] for each propagator are: $\Delta = 20$ ms $[-2.7\times10^{-4}:-2.9\times10^{-4}]$; $\Delta = 50$ ms $[-1.1\times10^{-3}:\ -8.8\times10^{-4}]$; $\Delta = 100$ ms $[-2.2\times10^{-3}:\ -2.2\times10^{-3}]$; $\Delta = 200$ ms $[-3.9\times10^{-3}:\ -4.7\times10^{-3}]$; $\Delta = 500$ ms $[-5.1\times10^{-3}:\ -0.015]$; $\Delta = 1{,}000$ ms $[6.2\times10^{-3}:\ -0.031]$.

simulation. Note the excellent agreement between experiment and simulation over a displacement scale that covers nearly four orders of magnitude. For the largest values of ζ the experimental propagators tend toward the Gaussian form, in agreement with earlier observations (Lebon et al., 1997).

In order to examine the effect of fluid self-diffusivity on dispersion, we carried out a simulation for a hypothetical fluid having the same velocity distribution in the pore space, but a much smaller self-diffusion coefficient ($D_s = 1.0\times10^{-10}$ m$^2\cdot$ s^{-1}) than water. This result is also shown in Figure 6. In the axial direction it is seen that at intermediate displacements ($0.1 \le \zeta \le 3$) the displacement variance is insensitive to the value of self-diffusivity used, demonstrating that dispersion is primarily determined by the properties of the medium, that is, mechanical or convective dispersion dominates. For small displacements ($\zeta \ll 0.1$), however, the displacement variance due to self-diffusion, which grows as $\sigma^2(t) \sim t$, dominates over mechanical dispersion, where $\sigma^2(t) \sim t^2$. An earlier study of the time-dependence of the dispersion characteristics of flow through similar bead packs (Manz et al., 1999) has shown that axial dispersion over lengthscales very much smaller than the pore size is characterized by Taylor dispersion in that the observed dispersion coefficient tends toward the self-diffusion coefficient of bulk water and σ^2 scales as t. On a scale smaller than an individual pore non-Fickian effects begin to become important, and on scales slightly larger than an individual pore ($\zeta \sim 1$) the dispersion is dominated by the geometry of the pore space. These results are therefore consistent with the observations presented here. For the

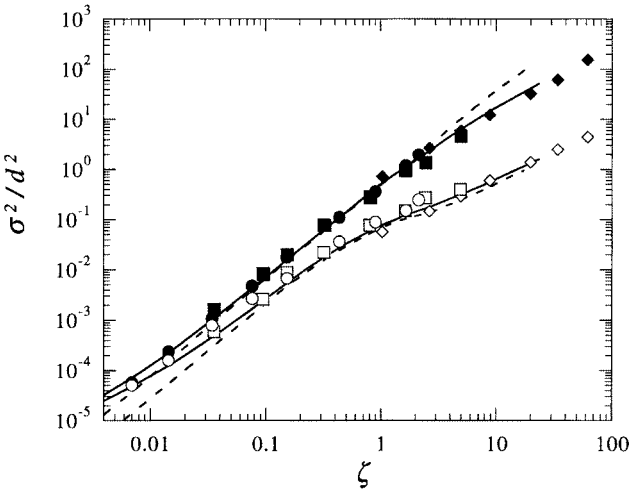

Figure 6. Normalized displacement variance as a function of the normalized average displacement for samples 1 (●, ○), 2 (■, □), and 3 (♦, ◇).

Filled and empty symbols represent the displacement variance in the axial and transverse directions respectively. The lattice-Boltzmann simulations are shown for $D_s = 2.2 \times 10^{-9}$ $m^2 \cdot s^{-1}$ (——) and $D_s = 1.0 \times 10^{-10}$ $m^2 \cdot s^{-1}$ (– – –) in the case of both axial and radial displacements.

case of transverse dispersion, Taylor dispersion appears to be important up to scales larger than that observed for the axial case since the lattice-Boltzmann simulations with the smaller diffusion coefficient underpredict the dispersion for $\zeta < 0.1$ (still smaller than the size of an individual pore), again in agreement with the results of Manz et al. (1999). Significant differences between the dispersion characteristics predicted using the two values of self-diffusivity over lengthscales characterized by $\zeta > 3$ are also observed. The effects of mechanical dispersion alone (probed in the simulations using the low value of self-diffusivity) overpredict the experimentally determined dispersion. This result is the subject of ongoing study, and at this stage we suggest that the differences between the results of the two lattice-Boltzmann simulations result from holdup phenomena within the bed. In earlier work, Sederman et al. (1997, 1998) have shown that regions of stagnant flow exist where the superficial flow meets a packing element within the bed. In the absence of diffusion, a fluid element entering such a stagnant region causes significant mechanical dispersion, as the difference in distance traveled, in the direction of the superficial flow, by fluid elements on nearby streamlines will increase with time. Diffusion of fluid from these stagnant regions to faster streams will decrease the dispersion. In this way the trends shown by the different lattice-Boltzmann simulations and the experimental data at large lengthscales can be explained. In constrast, in the transverse direction, mechanical dispersion appears to be the dominant contribution to σ^2 for $\zeta > 0.1$. It is also worth noting that for the largest displacement scales covered here ($\zeta > 10$) the axial displacement variance increases as $\sigma^2(\zeta) \sim \zeta^{\alpha}$, where $\alpha \approx 1.3$. As a consequence, the axial dispersion coefficient, which is given by $1/2\,(d\sigma^2/dt)$, does not reach its asymptotic limit on the time scales considered here. The origin of this effect could be due to holdup, as discussed earlier, or possibly systematic variations in the permeability within the bed; this is the subject of ongoing study. A similar effect has been reported by Lowe and Frenkel (1996), who carried out lattice-Boltzmann simulations of the velocity autocorrelation function within a computer-generated packing of spheres. It was found that the time decay of the velocity autocorrelation function was too slow to ensure convergence of D^*, which agrees with the data presented here.

Conclusions

In this study we have performed NMR velocimetry and propagator measurements, and lattice-Boltzmann simulations of the flow field within the same porous matrix. To achieve this, the matrix for the simulation was taken from a 3-D image of the pore space for which the flow phenomena were determined experimentally. Good quantitative agreement between flow visualization and the results of the lattice-Boltzmann simulation was found. Analysis of the velocity maps and axial displacement probability distributions suggested that large axial velocities are overpredicted by the simulation, while low velocities are underpredicted.

By introducing normalized parameters, the effect of mechanical dispersion over displacement scales extending over nearly four orders of magnitude was investigated. Excellent agreement was found between experimental results and the simulations for the normalized displacement variance in both the axial and transverse directions.

Given the quantitative agreement between the lattice-Boltzmann predictions and the magnetic resonance flow visualizations and measurements of dispersion, it was possible to investigate the extent to which mechanical dispersion dominated the dispersion characteristic of the flow, by varying the value of the self-diffusivity of the fluid used in the simulations. Dispersion was seen to be independent of the value of the fluid self-diffusivity used in the lattice-Boltzmann simulation over the normalized lengthscale ($0.1 \leq \zeta \leq 3$) suggesting that mechanical dispersion, that is, the inherent structure of the porous medium itself dominates the dispersion of the flow over these lengthscales and experimental conditions. At smaller lengthscales ($\zeta \ll 0.1$) the dispersion is determined by Taylor dispersion within individual pores, while at the largest lengthscales we suggest that holdup plays a significant role in the hydrodynamics characteristic of the porous medium.

Acknowledgments

One of the authors (L.F.G.) thanks EPSRC for the award of the NMR spectrometer. Another of the authors (B.M.) acknowledges the financial support of Unilever. The authors also thank P. Alexander and A. J. Sederman for their help in the final preparation of this manuscript.

Literature Cited

Aharanov, E., and D. H. Rothman, "Non-Newtonian Flow (Through Porous Media): A Lattice-Boltzmann Method," *Geophys. Res. Lett.*, **20**, 679 (1993).

Amin, M. H. G., S. J. Gibbs, R. J. Chorley, K. S. Richards, T. A. Carpenter, and L. D. Hall, "Study of Flow and Hydrodynamic Dispersion in a Porous Medium using Pulsed-Field-Gradient Magnetic Resonance," *Proc. R. Soc. Lond., A*, **453**, 489 (1997).

Baldwin, C. A., A. J. Sederman, M. D. Mantle, P. Alexander, and L.

F. Gladden, ''Determination and Characterisation of the Structure of a Pore Space from 3D Volume Images,'' *J. Colloid Interf. Sci.*, **181**, 79 (1996).
Behrend, O., R. Harris, and P. B. Warren, ''Hydrodynamic Behavior of Lattice Boltzmann and Lattice Bhatnagar-Gross-Krook Models,'' *Phys. Rev. E.*, **50**, 4586 (1994).
Calì, A., S. Succi, A. Cancelliere, R. Benzi, and M. Gramignani, ''Diffusion and Hydrodynamic Dispersion with the Lattice Boltzmann Method,'' *Phys. Rev. A*, **45**, 5771 (1992).
Callaghan, P. T., *Principles of Nuclear Magnetic Resonance Microscopy*, Clarendon Press, Oxford (1991).
Chen, H., S. Chen, and W. H. Matthaeus, ''Recovery of the Navier-Stokes Equations Using a Lattice-Gas Boltzmann Method,'' *Phys. Rev. A*, **45**, R5339 (1992).
Chen, S., F. Qin, K.-H. Kim, and A. T. Watson, ''NMR Imaging of Multiphase Flow in Porous Media,'' *AIChE J.*, **39**, 925 (1993).
Chen, S., and G. D. Doolen, ''Lattice Boltzmann Method for Fluid Flows,'' *Annu. Rev. Fluid Mech.*, **30**, 329 (1998).
Cotts, R. M., M. J. R. Hoch, T. Sun, and J. T. Marker, ''Pulsed Field Gradient Stimulated Echo Methods for Improved NMR Diffusion Measurements in Heterogeneous Systems,'' *J. Magn. Reson.*, **83**, 252 (1989).
Cushman, J. H., ''An Introduction to Hierarchical Porous Media,'' *Dynamics of Fluids in Hierarchical Porous Media*, J. H. Cushman, ed., Academic Press, San Diego (1990).
Cushman, J. H., *The Physics of Fluids in Hierarchical Porous Media: Angstroms to Miles*, Kluwer, Dordrecht, The Netherlands (1997).
Flekkøy, E. G., U. Oxaal, J. Feder, and T. Jøssang, ''Hydrodynamic Dispersion at Stagnation Points: Simulations and Experiments,'' *Phys. Rev. E*, **52**, 4952 (1995).
Frenkel, D., and M. H. Ernst, ''Simulation of Diffusion in a Two-Dimensional Lattice-Gas Cellular Automaton: A Test of Mode-Coupling Theory,'' *Phys. Rev. Lett.*, **63**, 2165 (1989).
Frisch, U., B. Hasslacher, and Y. Pomeau, ''Lattice-Gas Automata for the Navier-Stokes Equation,'' *Phys. Rev. Lett.*, **56**, 1505 (1986).
Georgiadis, J. G., D. R. Noble, M. R. Uchanski, and R. O. Buckius, ''Questions in Fluid Mechanics. Tortuous Micro-Flow in Large Disordered Packed Beds,'' *ASME J. Fluid Eng.*, **118**, 434 (1996).
Gonnella, G., E. Orlandini, and J. M. Yeomans, ''Lattice-Boltzmann Simulations of Complex Fluids,'' *Int. J. Mod. Phys. C*, **8**, 783 (1997).
Guilfoyle, D. N., P. Mansfield, and K. J. Packer, ''Fluid Flow Measurement in Porous Media by Echo-Planar Imaging,'' *J. Magn. Reson.*, **97**, 342 (1992).
Heijs, A. W. J., and C. P. Lowe, ''Numerical Evaluation of the Permeability and the Kozeny Constant for Two Types of Porous Media,'' *Phys. Rev. E*, **51**, 4346 (1995).
Higuera, F. J., and J. Jiménez, ''Boltzmann Approach to Lattice Gas Simulations,'' *Europhys. Lett.*, **9**, 663 (1989).
Kärger, J., and W. Heink, ''The Propagator Representation of Molecular Transport in Microporous Crystallites,'' *J. Magn. Reson.*, **51**, 1 (1983).
Kingdon, R. D., P. Schofield, and L. White, ''A Lattice Boltzmann Model for the Simulation of Fluid Flow,'' *J. Phys. A: Math. Gen.*, **25**, 3559 (1992).
Koch, D. L., and J. F. Brady, ''Dispersion in Fixed Beds,'' *J. Fluid Mech.*, **154**, 399 (1985).
Koch, D. L., and J. F. Brady, ''A Non-Local Description of Advection-Diffusion with Application to Dispersion in Porous Media,'' *J. Fluid Mech.*, **180**, 387 (1987).
Kutsovsky, Y. E., L. E. Scriven, H. T. Davis, and B. E. Hammer, ''NMR Imaging of Velocity Profiles and Velocity Distributions in Bead Packs,'' *Phys. Fluids*, **8**, 863 (1996).
Ladd, A. J. C., ''Numerical Simulations of Particle Suspensions via a Discretized Boltzmann Equation. Part 1. Theoretical Foundation,'' *J. Fluid Mech.*, **271**, 285 (1994).
Lebon, L., L. Oger, J. Leblond, J. P. Hulin, N. S. Martys, and L. M. Schwartz, ''Pulsed Gradient NMR Measurements and Numerical Simulation of Flow Velocity Distribution in Sphere Packings,'' *Phys. Fluids*, **8**, 293 (1996).
Lebon, L., J. Leblond, and J. P. Hulin, ''Experimental Measurement of Dispersion Processes at Short Times Using a Pulsed Field Gradient NMR Technique,'' *Phys. Fluids*, **9**, 481 (1997).
Lowe, C. P., and D. Frenkel, ''The Super Long-Time Decay of Velocity Fluctuations in a Two-Dimensional Fluid,'' *Physica A*, **220**, 251 (1995).
Lowe, C. P., and D. Frenkel, ''Do Hydrodynamic Dispersion Coefficients Exist?'' *Phys. Rev. Lett.*, **77**, 4552 (1996).
Maier, R. S., D. M. Kroll, Y. E. Kutsovsky, H. T. Davis, and R. S. Bernard, ''Simulation of Flow Through Bead Packs Using the Lattice Boltzmann Method,'' *Phys. Fluids*, **10**, 60 (1998).
Mansfield, P., and B. Issa, ''Fluid Transport in Porous Rocks. I. EPI Studies and a Stochastic Model of Flow,'' *J. Magn. Reson. A*, **122**, 137 (1996).
Manz, B., P. Alexander, and L. F. Gladden, ''Correlations Between Dispersion and Structure in Porous Media Probed by NMR,'' *Phys. Fluids*, **11**, 259 (1999).
Martys, N. S., and H. Chen, ''Simulation of Multicomponent Fluids in Complex Three-Dimensional Geometries by the Lattice Boltzmann Method,'' *Phys. Rev. E*, **53**, 743 (1996).
Mills, R., ''Self-Diffusion in Normal and Heavy Water in the Range 1−45°,'' *J. Phys. Chem.*, **77**, 685 (1973).
Packer, K. J., and J. J. Tessier, ''The Characterization of Fluid Transport in a Porous Solid by Pulsed Gradient Stimulated Echo NMR,'' *Mol. Phys.*, **87**, 267 (1996).
Paine, M. A., R. G. Carbonell, and S. Whitaker, ''Dispersion in Pulsed Systems—I,'' *Chem. Eng. Sci.*, **38**, 1781 (1983).
Qian, Y. H., D. d'Humières, and P. Lallemand, ''Lattice BGK Models for Navier-Stokes Equation,'' *Europhys. Lett.*, **17**, 479 (1992).
Rothman, D. H., and S. Zaleski, *Lattice-Gas Cellular Automata*, Cambridge Univ. Press, Cambridge (1997).
Salles, J., J.-F. Thovert, L. Delannay, J.-L. Auriault, and P. M. Adler, ''Taylor Dispersion in Porous Media. Determination of the Dispersion Tensor,'' *Phys. Fluids A*, **5**, 2348 (1993).
Sederman, A. J., M. L. Johns, A. S. Bramley, P. Alexander, and L. F. Gladden, ''Magnetic Resonance Imaging of Liquid Flow and Pore Structure Within Packed Beds,'' *Chem. Eng. Sci.*, **52**, 2239 (1997).
Sederman, A. J., M. L. Johns, P. Alexander, and L. F. Gladden, ''Structure-Flow Correlations in Packed Beds,'' *Chem. Eng. Sci.*, **53**, 2117 (1998).
Seymour, J. D., and P. T. Callaghan, '''Flow-Diffraction' Structural Characterization and Measurement of Hydrodynamic Dispersion in Porous Media by PGSE NMR,'' *J. Magn. Reson. A*, **122**, 90 (1996).
Seymour, J. D., and P. T. Callaghan, ''Generalized Approach to NMR Analysis of Flow and Dispersion in Porous Media,'' *AIChE J.*, **43**, 2096 (1997).
Shan, X., and H. Chen, ''Lattice Boltzmann Model for Simulating Flows with Multiple Phases and Components,'' *Phys. Rev. E*, **47**, 1815 (1993).
Shan, X., ''Simulation of Rayleigh-Bénard Convection Using a Lattice Boltzmann Method,'' *Phys. Rev. E*, **55**, 2780 (1997).
Spaid, M. A. A., and F. R. Phelan, Jr., ''Lattice Boltzmann Methods for Modeling Microscale Flow in Fibrous Porous Media,'' *Phys. Fluids*, **9**, 2468 (1997).
Stejskal, E. O., and J. E. Tanner, ''Spin Diffusion Measurements: Spin Echoes in the Presence of a Time-Dependent Field Gradient,'' *J. Chem. Phys.*, **42**, 288 (1965).
Tanner, J. E., ''Use of Stimulated Echo in NMR Diffusion Studies,'' *J. Chem. Phys.*, **52**, 2523 (1970).
Taylor, G., ''Dispersion of Soluble Matter in Solvent Flowing Slowly Through a Tube,'' *Proc. Roy. Soc. Lond. A*, **219**, 186 (1953).
Tessier, J. J., K. J. Packer, J.-F. Thovert, and P. M. Adler, ''NMR Measurements and Numerical Simulation of Fluid Transport in Porous Solids,'' *AIChE J.*, **43**, 1653 (1997).
Warren, P. B., ''Electroviscous Transport Problems via Lattice-Boltzmann,'' *Int. J. Mod. Phys. C*, **8**, 889 (1997).

Manuscript received Nov. 5, 1998, and revision received Apr. 8, 1999.